Assessment and discrimination of odor stimuli in rat olfactory bulb by dynamic functional MRI

Fuqiang Xu*†, Ikuhiro Kida‡, Fahmeed Hyder*, and Robert G. Shulman§

Departments of *Diagnostic Radiology, ‡Neurology, and §Molecular Biophysics and Biochemistry, Yale University, New Haven, CT 06510

Contributed by Robert G. Shulman, July 11, 2000

Dynamic blood oxygenation level-dependent functional MRI was applied at 7 T in the rat olfactory bulb (OB) with pulsed delivery of iso-amyl acetate (IAA) and limonene. Acquisition times for single-slice and whole OB data were 8 and 32 s, respectively, with spatial resolution of 220 × 220 × 250 μm. On an intrasubject basis, short IAA exposures of 0.6 min separated by 3.5-min intervals induced reproducible spatial activity patterns (SAPs) in the olfactory nerve layer, glomerular layer, and external plexiform layer. During long exposures (≈10 min), the initially dominant dorsal SAPs declined in intensity and area, whereas in some OB regions, the initially weak ventral/lateral SAPs increased first and then decreased. The SAPs of different concentrations were topologically similar, which implies that whereas an odor at various concentrations activates the same subsets of receptor cells, different concentrations are assessed and discriminated by variable magnitudes of laminar-specific activations. IAA and limonene reproducibly activated different subsets of receptor cells with some overlaps. Whereas qualitative topographical agreement was observed with results from other methods, the current dynamic blood oxygenation level-dependent functional MRI results can provide quantitative SAPs of the entire OB.

blood oxygenation level-dependent | functional mapping | olfactory bulb

In mammals, olfactory behaviors such as determination of food palatability and searching require accurate assessment and discrimination of different odor types, concentrations, and exposure duration (1). Distinctions between these behavioral tasks are believed to rely on a spatial-encoding mechanism in which different odor and concentrations evoke spatial activity patterns (SAPs) in the olfactory bulb (OB). The SAPs are derived from functionally induced activity in olfactory receptor neurons that synapse at specific glomeruli (2).

Insights into the coding of olfactory information have been partially inferred from SAPs in the OB, where the data can be obtained by various methods: 2-deoxyglucose autoradiography (3), electrophysiology (4), *c-fos* expression (5), functional MRI (fMRI) (6), and optical imaging of voltage-sensitive dyes (7) or intrinsic signals (8). Experimental limitations of each method affect data interpretations because each method maps a specific signal. Certain experimental criteria have to be met for olfactory perception to be systematically and ideally derived from the functional architecture revealed by the SAPs: (*i*) the neuroanatomy of the whole OB has to be mapped; (*ii*) the dynamic nature of SAPs in the whole OB has to be mapped with both high spatial and temporal resolutions; (*iii*) laminar-specific activations in the different layers have to be quantitated; and (*iv*) reproducibility of SAPs has to be established in a quantitative manner such that the effects of stimulus parameters (e.g., odor type, concentration, and exposure duration) can be easily identified and separated. If each criterion is met on an intrasubject basis by a particular methodology, that method then may be used for quantitative comparisons across subjects.

To this end, we applied the dynamic blood oxygenation level-dependent (BOLD) fMRI method (9) in a rat model with externally controlled odor presentation that delivered odor over a range of concentrations in a reproducible and pulsed manner. The fMRI method, in contrast to all other methods mentioned above, provides temporal patterns of SAPs from the whole OB where each frame in the movie contains olfactory processing information in five dimensions (i.e., three dimensions in space, one dimension in activity, and one dimension in time). Dynamic BOLD fMRI data reproducibly and quantitatively dissociate the effects of stimulus parameters (e.g., odor type, concentration, and exposure duration) on the SAPs on an intrasubject basis. Combination of high-spatial resolution conventional MRI and dynamic BOLD fMRI, in the same session, allowed anatomical and functional imaging, respectively, of the whole OB. The advantages of dynamic fMRI over other methods (e.g., noninvasive, repeated, intrasubject experiments of the whole OB with high spatial and temporal resolutions) have now been exploited to obtain five-dimensional information of the odor-elicited SAPs.

Materials and Methods

Animal Preparation. General details of the rat preparation for the olfactory experiments have been described (6) and approved by the Yale Animal Care and Use Committee (YACUC no. 7522). Male Sprague–Dawley rats (250–350 g) were anesthetized with 1–2% halothane and the skin overlying the OB was removed to expose the skull. A femoral artery was cannulated for monitoring blood pressure, gases, and pH levels throughout the experiment. Before the rat was placed into the magnet, the anesthesia was switched to urethane (i.p. 1.5 g/kg initial; 0.1 g/kg/h supplemental).

Odor Delivery. The entire odor delivery system was made of Teflon and glass with a dead volume of 20 ml. Mineral oil, which by itself did not produce any significant fMRI signal in control experiments, was used as the solvent to prepare odor solutions (4). The flow rate of the extra pure air (grade 0.1, <0.1 ppm hydrocarbon) passing over the odorant solution was kept at 5 liter/min, generating odorized airflow with 41, 520, and 4,500 ppm for iso-amyl acetate (IAA; Sigma) and 420 ppm for limonene (Fluka). The concentrations were calculated from the mass decrease of odorant over a period of 20 min under the experimental conditions. The odorized air was delivered through the nasal cavity by a ventilator with 3 ml/stroke at 60 stroke/min. The lung was ventilated separately to maintain the $p_{CO2} \approx 38$, $p_{O2} \approx 100$ mmHg, blood pH ≈ 7.4, and blood pressure ≈ 100 mmHg throughout the experiment.

Anatomical and fMRI. Imaging experiments were performed on a modified horizontal-bore 7T (Bruker, Billerica, MA) spectrom-

Abbreviations: BOLD, blood oxygenation level-dependent; fMRI, functional MRI; OB, olfactory bulb; ONL, olfactory nerve layer; GL, glomerular layer; EPL, external plexiform layer; SAP, spatial activity pattern; IAA, iso-amyl acetate; SNR, signal-to-noise ratio; *S*, prestimulation baseline image.

†To whom reprint requests should be addressed. E-mail: fuqiangxu@hotmail.com.

The publication costs of this article were defrayed in part by page charge payment. This article must therefore be hereby marked "*advertisement*" in accordance with 18 U.S.C. §1734 solely to indicate this fact.

Article published online before print: *Proc. Natl. Acad. Sci. USA*, 10.1073/pnas.180321397. Article and publication date are at www.pnas.org/cgi/doi/10.1073/pnas.180321397

eter. Images were obtained with the fast low-angle single-shot gradient-echo imaging sequence. The head was secured in a holder to minimize movement and the body temperature was maintained by a water-heated blanket (≈37°C). A circular radio-frequency transmit-receive surface coil probe (10-mm diameter) was centered on top of the skull above the OB. The magnetic field homogeneity was optimized (< 20 Hz) by coronal slice (5-mm thick) shimming.

The longitudinal relaxation time of tissue water-weighted fast low-angle single-shot anatomical images were obtained (image dimension = 128 × 128 pixels; in-plane resolution = 110 × 110 μm; slice thickness = 250 μm; repetition delay = 5.0 s; echo time = 16 ms; and flip angle = 60°) with variable inversion recovery weighting per slice. Each fMRI experiment consisted of a series of 128 apparent transverse relaxation time of tissue water-weighted fast low-angle single-shot images (image dimension = 64 × 64 pixels; in-plane resolution = 220 × 220 μm; slice thickness = 250 μm; repetition delay = 25–125 ms; echo time = 16 ms; and flip angle = 5–15°). In each experiment, 16 dummy scans per slice were carried out before data acquisition. The temporal resolutions were 8 s per image and 1.5 s per image for single- and 20-slice experiments, respectively.

Stimulation Protocols. Typically two types of stimulation protocols were used: (*i*) a train of short exposures of 0.6-min with a fixed interstimulation interval of 3.5 min; and (*ii*) the combination of a single 0.6-min exposure followed by a long exposure (≈10 min) with an interstimulation interval similar as in *i*. The experiments with short exposures were always performed before the long exposures with 15 min of breathing moisturized air between successive experiments. In each experiment, eight or 16 "baseline" images were acquired, during which the rats breathed moisturized pure air.

fMRI Data Processing. Details of data processing have been described (6, 10). Briefly, after conversion of sequentially sampled data and two-dimensional Fourier transformation (11), head movement artifacts were assessed by a center-of-mass analysis. Images were discarded from analysis if the center-of-mass deviation was greater than 25% of a pixel size. For each experiment, the mean image of the prestimulation "baseline" images (S) was subtracted from the "stimulation" images ($\Delta S + S$) on a pixel-by-pixel basis to produce either $\Delta S/S$ maps or Student's t maps. Usually, 2–4 functional maps were averaged to give a single functional map. Each linearly interpolated t map was overlaid onto the corresponding anatomical image to form the SAPs in the whole OB, which revealed the location of activity in the bulbar layers: the olfactory nerve layer (ONL), glomerular layer (GL), and external plexiform layer (EPL). Layer segmentation in the rat OB is based on the contrast-to-noise ratio across layers, which are similar in magnitude of contrast-to-noise in anatomical images of the human brain that distinguish gray from white matter (10). The MRI layer segmentation is based on *a priori* information from histological staining (12). Because varied longitudinal relaxation time of tissue water contrast was depicted in different slices, the contrast-to-noise for visualization of bulbar layers in certain slices were better than others.

Time courses of SAPs were plotted for particular regions of interest to reveal dynamic patterns of $\Delta S/S$. For the analysis of difference in SAPs elicited by different odor stimuli, linear Pearson correlation coefficients between paired functional maps were calculated based on spatially binned data. Similarly, Spearman's rank correlation coefficients were calculated for the analysis of similarity between regions of interest.

Results

Reproducibility and Neuroanatomy of SAPs. For the SAP to code olfactory information, it must be reproducible in repeated exposures. Fig. 1*A* shows that in the same rat, the SAPs were very reproducible with 0.6-min odor stimulations. The general features of the SAPs were conserved in different exposures across the slice. In the most activated dorsolateral focus, as indicated by a circle in Fig. 1*A*, the pattern showed high reproducibility as shown in Fig. 1*B* (Spearman's rank correlation coefficients for rat 1: $r_{1st\ vs.\ 2nd} = 0.72$, $P < 0.001$; $r_{2nd\ vs.\ 3rd} = 0.74$, $P < 0.001$; and $r_{3rd\ vs.\ 4th} = 0.71$, $P < 0.001$). Fig. 1*C* shows that intensities of the SAPs that are spatially reproducible (Fig. 1*B*) decreased slightly with repeated exposures. The increase and decrease of odor-elicited $\Delta S/S$ changes correlated well with the onsets and offsets of stimulation. Decay of the signal after offset was always longer (by ≈8 s) than the signal rise delay, presumably from slow odor clearance at the epithelium (13).

To investigate any dependence of OB activities on the duration of odor exposures, we compared SAPs generated with short and long exposures in the same rat. Fig. 2*A* shows the single-slice SAPs acquired during 0.6- and 10-min exposures, and Fig. 2*B* shows the response time courses of two foci during the experiment. In Fig. 2*A*, the first two images, under similar conditions as the first two exposures in Fig. 1, show high reproducibility of SAPs and a slight intensity decrease. The initial 0.6-min period of the 10-min exposure produced strong dorsal-lateral and weaker ventral activations, as in the first short 0.6-min exposure (Fig. 2*B*), again similar to the first two exposures in Fig. 1. Because the exposure was prolonged, however, the dorsolateral activation decreased continuously in area and intensity, whereas the ventrolateral activations gradually increased in area and intensity in the first 4 min, and then fell off slightly over time. In the first 0.6 min of the 10-min exposure, there were 10 pixels that reached a threshold of $P < 0.01$ in the dorsal-lateral focus (*a* in the inset of Fig. 2*B*). By $t = 9$ min, there were no pixels above that threshold in the same dorsal-lateral focus. In contrast, the area in the lateral focus (*b* in inset of Fig. 2*B*), increased from 0 pixels at 0.6 min to 8 pixels at 4 min, and decreased to 5 pixels at 9 min at a threshold of $P < 0.01$. The response properties of different OB regions clearly varied with exposure duration.

Bulbar functions are segregated by layers; therefore, it is important to reveal the layered location of the BOLD signals. In Fig. 1, single-slice data show that the SAPs induced by 520 ppm IAA are primarily localized within the GL, extending into neighboring ONL and EPL. The SAPs in the two OBs were laterally asymmetric per slice, which possibly could be attributed to individual variations such as air intake capabilities of each nostril. In all cases examined ($n = 8$), planar asymmetries were much larger than intra-animal experimental variations. Generally, the SAPs in anterior and posterior slices were located dorsolaterally and ventromedially, respectively. These functional neuroanatomical findings of laminar-specific SAPs caused by IAA exposure in whole rat-OB are generally consistent with our previous fMRI study (6) in that large BOLD signal changes were observed in the ONL, which contains tightly packed unmyelinated axons and glial cells.

Effects of Odor Concentrations on SAPs. Animals can discriminate a broad range of odorant concentration (14). Whole-bulb SAPs from the same rat at different IAA concentrations (41, 520, and 4,500 ppm) are demonstrated in Fig. 3. The first three columns show the SAPs at three concentrations, thresholded at the same value ($P < 0.04$). The fourth column shows the same data of the first column thresholded lower ($P < 0.18$), revealing more voxels. The patterns evoked at the low concentration with low probability are topologically similar to those evoked at high concentration with high probability.

For a particular focus, which is circled in slice 5 of Fig. 3, the specific SAPs at different concentrations are shown in Fig. 4*A* thresholded at $P < 0.04$ (4,500 ppm), $P < 0.10$ (520 ppm), and $P < 0.20$ (41 ppm). The high-spatial correlation of the activated

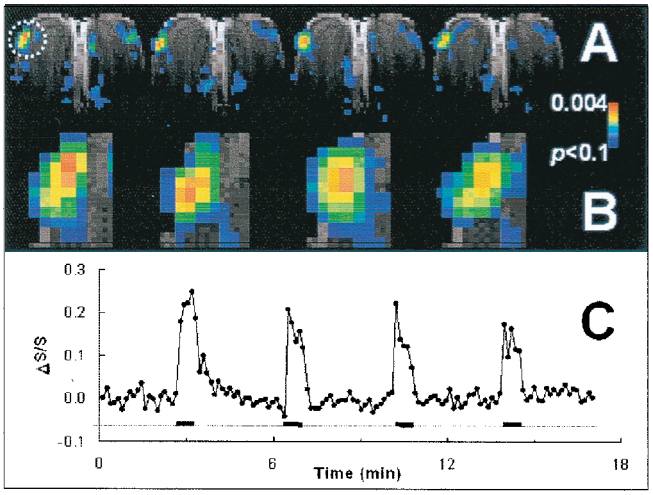

Fig. 1. Odor-elicited SAPs and corresponding time courses of $\Delta S/S$ during four repeated exposures in the same rat. (*A*) SAPs of rat exposed to 520 ppm IAA (rat one, total of eight rats). (*B*) Enlarged SAPs of the highly activated focus shown in *A* by the circle. (*C*) Time course of $\Delta S/S$ (line with solid circles) with the entire experimental run, with four 0.6-min repeated exposures (thick black line) with 3.5-min intervals of pure air (dotted line). See *Results* for further details.

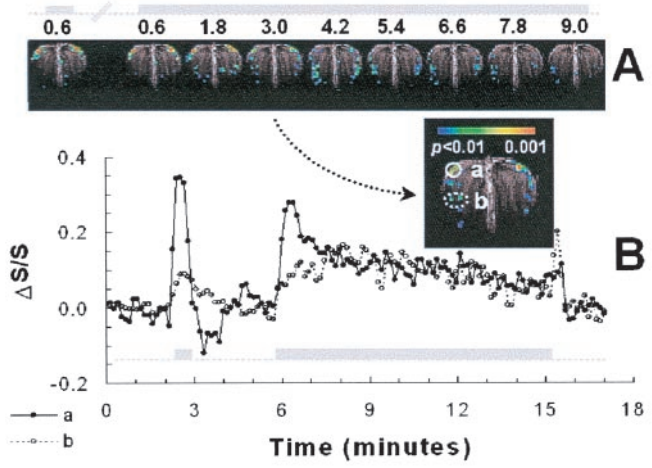

Fig. 2. Odor-elicited SAPs and corresponding time courses of $\Delta S/S$ in consecutive short and long exposures to 520 ppm IAA in the same rat (rat two, total of five rats). (*A*) SAPs generated with short and long exposures of IAA. The time course of the odor exposure is shown above the images in gray. (*B*) Time course of $\Delta S/S$ in foci *a* and *b* (see inset). See *Results* for further details.

region of interest at the different concentrations is evident, although slight variations of the hot spots within the regions of interest are observed (Fig. 4*A*). The center-of-mass for a 5×5 pixel area was highly correlated at the different concentrations (Spearman's rank correlation coefficients: $r_{41 \text{ vs. } 520 \text{ ppm}} = 0.82$, $P < 0.001$; $r_{41 \text{ vs. } 4500 \text{ ppm}} = 0.67$, $P < 0.001$; $r_{520 \text{ vs. } 4500 \text{ ppm}} = 0.72$, $P < 0.001$), indicating that the hot spots were similar, in terms of location and intervoxel intensity. Fig. 4*B* shows the same data as in Fig. 4*A* but with a threshold of $P < 0.04$ for all concentrations. The $\Delta S/S$ and activated area revealed in Fig. 4*B* are plotted vs. IAA concentrations in Fig. 4*C*. The average intensity of the 25 pixels correlated well with the odorant concentration (Pearson's correlation coefficients for the 5×5 pixels: $r_{41 \text{ vs. } 520 \text{ ppm}} = 0.82$, $P < 0.001$; $r_{41 \text{ vs. } 4,500 \text{ ppm}} = 0.67$, $P < 0.001$; and $r_{520 \text{ vs. } 4,500 \text{ ppm}} = 0.72$, $P < 0.001$), although there was some falling off from linearity at higher concentrations (Fig. 4*C*). The BOLD signal changed by a factor of $\approx$3 whereas the activated area (at the same threshold of $P < 0.04$) increased by a factor of $\approx$20 over a concentration change of $\approx$100. The BOLD signal and area increases were monotonic for the three concentrations measured.

SAPs of Different Odors. Odors with different chemical structures have different receptor affinity profiles in the olfactory epithelium (15). Fig. 5 compares the SAPs generated by two odors, IAA and limonene in a single slice with three repeated 0.6-min exposures. Similar to the results shown in Fig. 1, the SAP of each odorant was highly reproducible for repeated stimuli, except that the intensity decreased with repeated exposure. These two odorants produced patterns that were clearly distinct, and their differences were much greater than the variations between different SAPs with repeated exposures of the same odorant. Some pixels were activated by both odors, whereas some pixels were activated to significant levels by only one of them. The observation of different SAPs between two odors was in accord with optical mapping of the antennal lobe of the honeybee (16), salamander (7), fish (17), and the dorsal region of the rat OB (8).

Discussion

SAPs in the rat OB elicited by IAA and varying with exposure periods and concentrations were visualized by using BOLD fMRI with high spatial and temporal resolutions. The highly activated foci were mainly centered in the GL with definite but smaller activations in the ONL and EPL. In the same animal, the SAPs were very reproducible with short exposures, whereas gradual changes at specific locations evolved with prolonged exposure. The intensities of the SAPs increased with odorant concentration; however, the patterns at different concentrations were topologically similar. Different odorants created overlapping but specific SAPs differing significantly in the same rat. The SAPs with exposures of an odor were significantly more similar than the SAPs with exposures of two odors.

SAPs Are Highly Reproducible with Brief Exposures. Short exposures of 0.6 min with 3.5-min intervals demonstrated the high reproducibility of SAPs. Adaptation in which the signal intensity decreased after stimulations whereas the activated area remained quite constant occurred in the OB (Fig. 1). Many mechanisms of desensitization, adaptation, and habituation on different anatomical levels have been reported in the olfactory system (for example, see refs. 18–20). Because of the different animals models, methods, and response times, no assignment of mechanism to our observation is possible on this basis. The observed time course of $\approx$1 min for this widespread and close to uniform decrease in amplitude of individual voxel could be caused by the adaptation in both epithelium and/or OB.

Modification of SAPs with Prolonged Exposure. Although the SAPs elicited with short exposures are highly reproducible (Fig. 1), the intensities of the early activated pixels decreased and some others increased with longer exposure times, evolving new patterns (Fig. 2). The slow increase in lateral activity could be caused by the products of nasal chemical reactions catalyzed by various enzymes (21). Previous research has shown that the chemical reactions in the nasal cavities are capable of breaking down the odor molecules into smaller molecules (22). In the current study, the odorant, an ester, could be hydrolyzed into alcohol and carboxylic acid by esterases known to exist in mucus. Therefore, the increased lateral SAPs could be caused by the accumulation of these products over time. Alternatively, the increased lateral and/or decreased dorsal activations may be attributed to varied accessibility of odor molecules to receptor neurons in different locations within the nasal cavity (23),

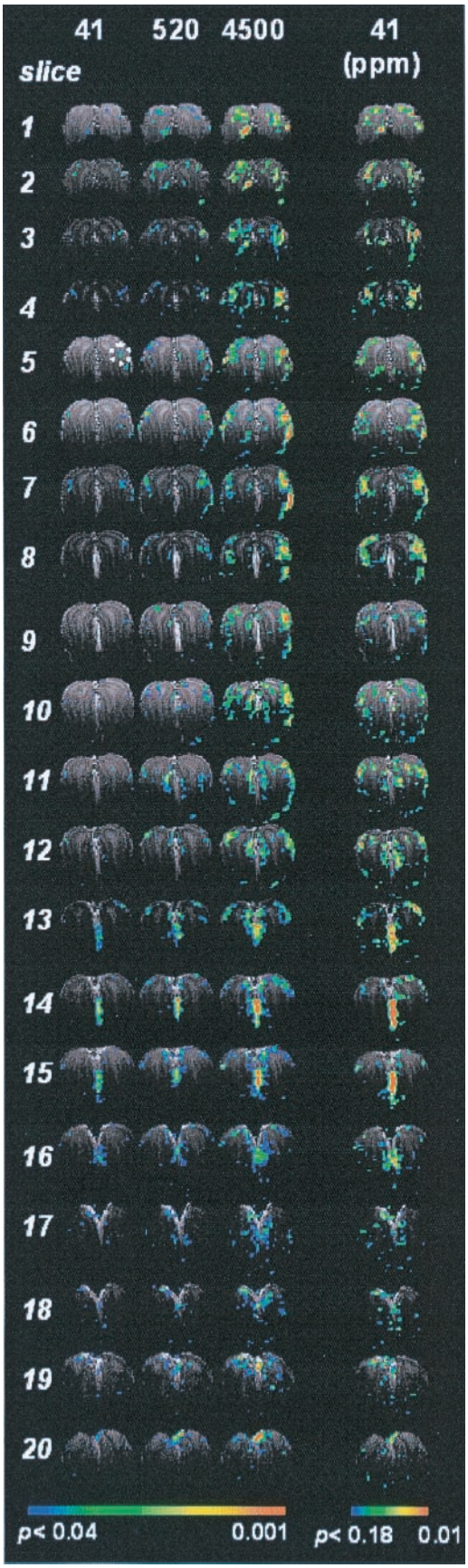

Fig. 3. The effect of odorant concentration on SAPs: the variability of activation intensity and the invariability of the SAPs across the OB. Each image represented summed response of the two frames acquired during the 64-s exposure to different concentrations of IAA (41, 420, and 4,500 ppm) in the same rat (rat three, total of four animals). All images in columns 1–3 were thresholded at the same value ($P < 0.04$), whereas the images in column 4, the same set of data in column 1, were thresholded at $P < 0.18$. The slices were displayed from anterior (slice no. 1) to posterior (slice no. 20). The high activity located between the two OBs in slices 13–16 is not reproducible among rats and therefore might be caused by artifacts.

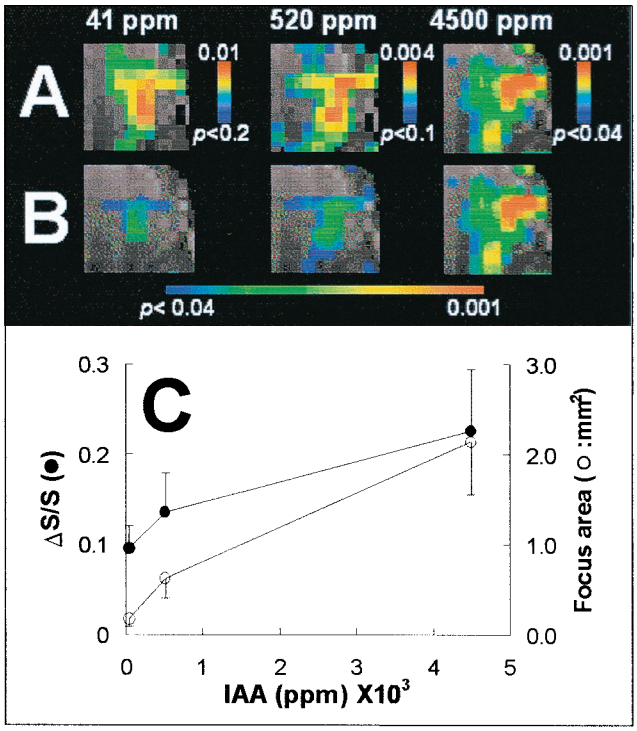

Fig. 4. The effect of odorant concentration on SAPs. (*A*) The topographical invariability and intensity variability of the SAPs in highly activated foci at different concentrations. The focus was in slice 5 indicated by a circle in column 1 of Fig. 3. (*B*) The effect of concentration on the area and intensity of the focus. The intensity is the averaged BOLD signal of the focus and the area is the focus (5×5 pixels) reached the threshold ($P < 0.04$). The values are means ± SD ($n = 3$).

inhibition of the activated glomerulus to its surrounding glomeruli (24), and/or central feedback into the OB from higher brain regions (25).

High Activity in the ONL. Our results showed that the highly activated foci extended well into ONL (for example, slices 5–16 in Fig. 3). Furthermore, in some regions, the ONL contained high activity even when the adjacent GL was not activated (see the lateral regions in slices 5–8 of Fig. 3). The ONL activations indicate high-energy consumption in that layer and localization of this activity is not inconsistent with the functional anatomy of olfactory nerves. The axons from different types of olfactory receptor neurons form olfactory nerve bundles, and on the way from epithelium through cribriform bone to their targets in the OB, they regroup to form more homogenous bundles (26). Each bundle contains ≈50 axons that are ensheathed by glial cells. Because these axons are among the thinnest in the body, unmyelinated and tightly packed, significant amounts of energy may be needed for ion pumping, thus explaining the strong BOLD signal changes in the ONL. Because BOLD signal changes recently have been associated with energy consumption

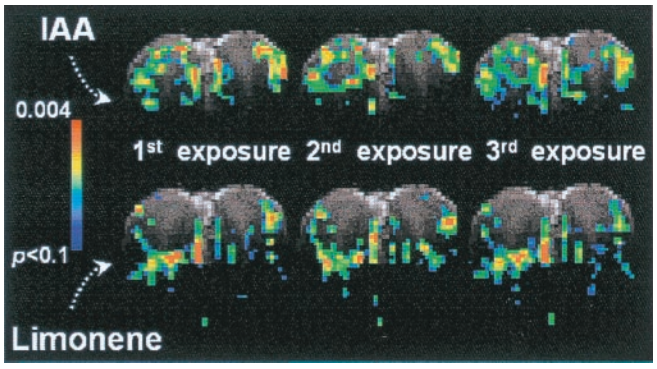

Fig. 5. SAPs elicited by IAA and limonene in the same rat (rat four, total of three rats). The concentrations are 520 and 420 ppm for IAA and limonene, respectively. The SAPs are reproducible for the same odorant in repeated exposures but different for different odorant.

(27), the high activations observed in the ONL correspond to elevated energetic demands of the nerve fibers during stimulation. 2-Deoxyglucose mapping has shown similar ONL activations (3). Mapping data from methods that cannot distinguish laminar structures of the OB must be interpreted with caution.

Glomeruli Form Functional Clusters. Activation of glomerular clusters has been observed in response to an odorant. This suggests that the organization of glomeruli follows some rules such that the activity patterns are logical/simple rather than randomly distributed hot spots across the OB. Our data shows that SAPs are composed of activated foci, which are broadly distributed in the OB (Fig. 3), indicating that one odorant is able to activate many subtypes of receptor neurons. The largest cluster located at the lateroanterior OB is $\approx$1 mm^2 at high concentrations ($P <$ 0.01), appearing in several slices and covering scores of voxels and up to 100 glomeruli (assuming the average size of rat glomerulus is 100 μm). These observations seem related to two categories of recent studies—receptor neurons expressing similar receptor proteins projecting to adjacent glomeruli (28) and a cluster of glomeruli activated by homologous odorants (29, 30). Of course, the underlying assumption associating these two categories is that an odorant activates neurons expressing similar receptors (31), hence, adjacent glomeruli. The structure-function relationships of receptor proteins suggest that if an odorant strongly stimulates a glomerulus, it is likely to stimulate adjacent glomeruli (although to different levels), forming an activated cluster in the GL.

Intrasubject cluster data for different odors (Fig. 5) advances the quantitative understanding of the topics raised above, because comparisons of 2-deoxyglucose clusters from different odors can only be obtained from different animals. Our results in the same rat showed that IAA and limonene elicited overlapping but different SAPs. Because the activity of these glomeruli is the summation of responses from specific receptor neurons, and each receptor protein has a specific binding pocket, the convergence of one subtype of neurons to a few glomeruli transforms the glomerular layer of the OB into an array of elements that recognize different chemical structures.

The Tensor Model. Clearly, SAPs from specific odorants are represented by five-dimensional parameters in the OB. We have explored the time dimension within some limits (e.g., Figs. 1 and 2), although much more remains to be investigated and even higher temporal resolution is available from fMRI. Here, we set aside temporal concerns and concentrate on the remaining four dimensions, i.e., Cartesian coordinates of space and the amplitude axis of response. The SAPs, which have been generated here with spatial and amplitude information completely intact, are suited for an interpretation in which each odorant stimulates a number of glomeruli with characteristic amplitudes. We assume that the ratio of the amplitudes from the different glomeruli within a SAP identifies and characterizes the odorant (i.e., interglomeruli activity allows the "recognition" of an odorant), and these amplitudes vary with experimental conditions such as odorant concentrations, acquisition sensitivity, etc [i.e., experimental factors that affect the signal-to-noise ratio (SNR) of olfactory processing]. There are $\approx$2,000 glomeruli in each bulb, and after the usual assumptions in the field that the SAP for a range of i different odors can be represented in the OB by a linear combination of the glomerulus space, G_j, with an activity-connectivity tensor, A_{ij} (where $0 < j \leq 2{,}000$ and $1 \leq i \ll \infty$). Then the SAP for concentration c can be represented by a relationship

$$S_c = A_{ij}\, G_j \qquad [1]$$

This type of population coding has been proposed as a mechanism for signal processing in the OB and olfactory and visional cortices (32–35) and it should be particularly useful for determining solutions in closed form because of the finite number of glomeruli. The large dimensionality in glomerular space has the advantage of being quantified. Assuming that within the dynamic range, each glomerulus has the same dosage-response properties, the effects of odorant concentrations on A_{ij} in G_j Eq. **1** can be scaled by N at concentration d:

$$S_d = NS_c \qquad [2]$$

where N varies with conditions such as concentration or receiver gain (i.e., for $d = c$, $N = 1$). In this study, the SAPs are generated either as $\Delta S/S$ which is the fundamental change of the BOLD signal or as p values representing the likelihood that the activation is accidental. In both presentations, contributions to the SAP are plotted only when the amplitudes are larger than the rms noise by some threshold value. Some elements in A_{ij} may vanish as concentrations drop or other conditions that lower SNR (e.g., compare lowest and highest concentrations in Fig. 4*B*). A smell is "recognized" over a range of odorant concentrations. "Recognition" of odor intensity presumably results from the amplitudes of significantly activated glomeruli transmitted to the higher olfactory centers in the brain. The data in Figs. 3 and 4 showed that the different concentrations of the same odorant generate SAPs that are different in amplitudes but similar in topography. These results support the model on the spatial resolution of our voxel level, which contains 4–8 full glomeruli.

Theoretical correlations between the SAPs and the cortical response(s) are quantitated to understand the processing of olfaction. Hopfield (33) has emphasized that beyond the OB mapping there are complex questions that are involved in odor identification, such as odor memory, temporal responses, and separation of components within a mixture. The relationships of Eqs. **1** and **2** ultimately demonstrated above require that the BOLD signal must be converted to neuronal firing. This conversion can be accomplished through converting the BOLD signal to energy consumption (27) and thereby to neuronal firing (36). By using higher spatial resolution fMRI, the model can be tested further on the glomerular level. Although many challenges remain, we are on a path to further understanding olfactory processing.

Quantitative Coding of Olfactory Information. Most animals can discriminate a broad range of odorant concentrations (14, 37). It has been recently hypothesized that different concentrations may yield different SAPs through "recruitment" (8). In biology, the term "recruitment" is used when additional functional units

(e.g., capillaries, neurons, pathways, etc.) are used compared with control conditions. By varying the threshold, higher and lower concentrations of an odor generate SAPs that are topologically similar but with different amplitudes (Figs. 3 and 4*A*), providing the basis for the assumption of Eq. (2). The simplest explanation of the stronger activation at high concentrations would be increased activation of receptor neurons by higher ligand binding.

The results shown in Figs. 3 and 4 indicate that within a range an odor has a specific activity pattern that does not depend on odorant concentration, and therefore, recruitment of more receptor neurons (i.e., more glomeruli) with higher concentration as recently suggested (8) is not supported by these results. High SNR allows us to compare SAPs of different concentration at low threshold. Without this high SNR, we would see that previously unexcited voxels were recruited at high concentrations (Fig. 4*B*). The pattern change with thresholding (Fig. 4*A*) demonstrates the dependence of recruitment on SNR. For weaker signals, it could be claimed to exist, as has been done from optical reflectance data of the OB (8). With higher SNR, as in these experiments, recruitment is not observed. As we have discussed before, in conjunction with fMRI of the auditory response in humans, the concept of ''recruitment'' is coupled to SNR and can only be unambiguously claimed to exist if the experiment had infinite SNR (38).

Conclusions

We have succeeded in visualizing the odor-elicited SAPs in the whole rat-OB with high spatial resolution. For short-repeated exposures, the SAPs were highly reproducible, with strongest activity located in the GL. In specific regions, significantly different SAPs evolved with prolonged odor exposure. Although the activity in the OB increased with odorant concentration, the patterns at different concentrations were similar topologically. IAA and limonene created overlapping but significantly different SAPs. These results agree with the concept that SAPs in the OB code olfactory information. fMRI as a noninvasive method that is capable of providing five-dimensional information about the patterns in the same animal for repeated exposures of the same and/or different odors will be a powerful tool to study not only the activity patterns in the OB but also the information processing in the higher olfactory centers in the brain.

We thank the Yale Magnetic Resonance Center technical staff, Mrs. P. Brown, S. McIntyre, and T. Nixon for maintenance of the spectrometer and Drs. G. M. Shepherd, D. L. Rothman, X. Yang, V. Lebron, and A. Rangarajan for helpful discussions. This work was supported by grants from the National Institutes of Health (DC-003710 to R.G.S. and NS-37203 to F.H.) and National Science Foundation (DBI-9730892 to F.H.).

1. Doty, R. L. (1986) *Experientia* **42,** 257–271.
2. Hildebrand, J. G. & Shepherd, G. M. (1997) *Annu. Rev. Neurosci.* **20,** 595–631.
3. Sharp, F. R., Kauer, J. S. & Shepherd, G. M. (1975) *Brain Res.* **98,** 596–600.
4. Mori, K. (1995) *Curr. Opin. Neurobiol.* **5,** 467–474.
5. Guthrie, K. M. & Gall, C. M. (1995) *Chem. Senses* **20,** 271–282.
6. Yang, X., Renken, R., Hyder, F., Siddeek, M., Greer, C. A., Shepherd, G. M. & Shulman, R. G. (1998) *Proc. Natl. Acad. Sci. USA* **95,** 7715–7720.
7. Cinelli, A. R. & Kauer, J. S. (1995) *J. Neurophysiol.* **73,** 2033–2052.
8. Rubin, B. D. & Katz, L. C. (1999) *Neuron* **23,** 499–511.
9. Ogawa, S., Lee, T. M., Nayak, A. S. & Glynn, P. (1990) *Magn. Reson. Med.* **14,** 68–78.
10. Hyder, F., Phelps, E. A., Wiggins, C. J., Labar, K. S., Blamire, A. M. & Shulman, R. G. (1997) *Proc. Natl. Acad. Sci. USA* **94,** 6989–6994.
11. Hyder, F., Rothman, D. L. & Blamire, A. M. (1995) *Magn. Reson. Imaging* **13,** 97–103.
12. Greer, C. A., Stewart, W. B., Kauer, J. S. & Shepherd, G. M. (1981) *Brain Res.* **217,** 279–293.
13. Getchell, T. V., Margolis, F. L. & Getchell, M. L. (1984) *Prog. Neurobiol.* **23,** 317–345.
14. Schild, D. (1988) *Biophys. J.* **54,** 1011.
15. Scott, J. W., Brierley, T. & Schmidt, F. H. (2000) *J. Neurosci.* **20,** 4721–4731.
16. Joerges, J., Kuttner, A., Galizia, C. G. & Menel, R. (1997) *Nature (London)* **387,** 285–288.
17. Friedrich, R. W. & Korsching, S. I. (1998) *J. Neurosci.* **18,** 9977–9988.
18. Leinders-Zufall, T., Ma, M. & Zufall, F. (1999) *J. Neurosci.* **19,** RC19.
19. Nickell, W. T. & Shipley, M. T. (1993) *J. Neurosci.* **13,** 650–659.
20. Wachowiak, M. & Cohen, L. B. (1999) *J. Neurosci.* **19,** 8808–8817.
21. Dahl, A. R. & Hadley, W. M. (1991) *Crit. Rev. Toxicol.* **21,** 345–372.
22. Stott, W. T. & McKenna, M. J. (1984) *Fundam. Appl. Toxicol.* **4,** 594–602.
23. Cleland, T. A. & Linster, C. (1999) *Neural Comput.* **11,** 1673–1690.
24. Imamura, K., Mataga, N. & Mori, K. (1992) *J. Neurophysiol.* **68,** 1986–2002.
25. Ciombor, K. J., Ennis, M. & Shipley, M. T. (1999) *Neuroscience* **90,** 595–606.
26. Daston, M. M., Adamek, G. D. & Gesteland, R. C. (1990) *Brain Res.* **537,** 69–75.
27. Kida, I., Kennan, R. P., Rothman, D. L., Behar, K. L. & Hyder, F. (2000) *J. Cereb. Blood Flow Metab.* **20,** 847–860.
28. Tsuboi, A., Yoshihara, S., Yamazaki, N., Kasai, H., Asai-Tsuboi, H., Komatsu, M., Serizawa, S., Ishii, T., Matsuda, Y., Nagawa, F., *et al.* (1999) *J. Neurosci.* **19,** 8409–8418.
29. Mori, K. & Shepherd, G. M. (1994) *Semin. Cell. Biol.* **5,** 65–74.
30. Johnson, B. A., Woo, C. C., Hingco, E. E., Pham, K. L. & Leon, M. (1999) *J. Comp. Neurol.* **409,** 529–548.
31. Malnic, B., Hirono, J., Sato, T. & Buck, L. B. (1999) *Cell* **96,** 713–723.
32. Pellionisz, A. & Llinas, R. (1979) *Neuroscience* **4,** 323–348.
33. Hopfield, J. J. (1999) *Proc. Natl. Acad. Sci. USA* **96,** 12506–12511.
34. Tanaka, K., Saito, H., Fukada, Y. & Moriya, M. (1991) *J. Neurophysiol.* **66,** 170–189.
35. Rolls, E. T., Critchley, H. D. & Treves, A. (1996) *J. Neurophysiol.* **75,** 1982–1996.
36. Shulman, R. G. & Rothman, D. L. (1998) *Proc. Natl. Acad. Sci. USA* **95,** 11993–11998.
37. Laing, D. G. (1986) *Physiol. Behav.* **37,** 163–170.
38. Dhankhar, A., Wexler, B. E., Fulbright, R. K., Halwes, T., Blamire, A. M. & Shulman, R. G. (1997) *J. Neurophysiol.* **77,** 476–483.